crystals

MDPI

Article

Synthesis of a Novel Zinc(II) Porphyrin Complex, Halide Ion Reception, Catalytic Degradation of Dyes, and Optoelectronic Application

Soumaya Nasri [1,2,*], Mouhieddinne Guergueb [2], Jihed Brahmi [2], Youssef O. Al-Ghamdi [1], Frédérique Loiseau [3] and Habib Nasri [2]

[1] Department of Chemistry, College of Science Al-Zulfi, Majmaah University, Majmaah 11952, Saudi Arabia
[2] Laboratory of Physical Chemistry of Materials, Faculty of Sciences of Monastir, University of Monastir, Avenue de l'environnement, Monastir 5019, Tunisia
[3] Département de Chimie Moléculaire, 301 rue de la Chimie, Université Grenoble Alpes, CS 40700, CEDEX 9, 38058 Grenoble, France
* Correspondence: soumaya.n@mu.edu.sa

Abstract: This work describes the synthesis of a novel zinc(II) porphyrin complex, namely [*Meso*-4α-tetra-(1,2,3-triazolyl)phenylporphyrinato]zinc(II) symbolized by 4α-[Zn(TAzPP)] (**4**), using the click chemistry approach in the presence of copper iodide. All of the synthetic porphyrin species reported herein were fully characterized by elemental analysis, infrared spectroscopy, proton nuclear magnetic resonance, UV-visible spectroscopy, and fluorescence. To synthesize the 4α-[Zn(TAzPP)] complex (**4**), we produced 4α-*Meso*-tetra-*o*-nitrophenylporphyrin ($H_2T_{NO2}PP$) and 4α-*meso*-tetra-*o*-aminophenylporphyrin (4α-H_2TNH_2PP) (**1**) using known classic literature methods. This 4α atropisomer was converted to 4α-*meso*-tetra-*o*-azidophenylporphyrin (4α-H_2TN_3PP) (**3**) by reaction with sodium nitrite and sodium azide, and then it was metalated by Zn(II), leading to [4α-*meso*-tetra(2-azidophenyl)porphyrinate]zinc(II) (4α-[Zn(TN_3PP)]) (**3**). The click chemistry synthetic method was finally used to prepare 4α-[Zn(TAzPP)] (**4**). This new tetracoordinated zinc(II) porphyrin complex was prepared and characterized in order to: (i) produce a receptor for anion recognition and sensing application for Cl^- and Br^-; (ii) study the catalytic decomposition of rhodamine B (RhB) and methyl orange (MO) dyes; and (iii) determine the electronic characteristics as a photovoltaic device. Complex (**4**) formed 1:1 complex stoichiometric species with chloride and bromide halides and the average association constants of the 1:1 addicts were ~ 10^3. The photodecomposition of RhB and MO dyes in the presence of complex (**4**) as a catalyst and molecular oxygen showed that complex (**4**) presented a photodegradation yield of approximately 70% and could be reused for five successive cycles without any obvious change in its catalytic activity. The current-voltage characteristics and impedance spectroscopy measurements of complex (**4**) confirmed that our zinc(II) metalloporphyrin could be used as a photovoltaic device.

Keywords: zinc(II) porphyrins; click chemistry; optical anion sensing; UV-visible titration; photoelectronic degradation; photovoltaic devices

check for updates

Citation: Nasri, S.; Guergueb, M.; Brahmi, J.; O. Al-Ghamdi, Y.; Loiseau, F.; Nasri, H. Synthesis of a Novel Zinc(II) Porphyrin Complex, Halide Ion Reception, Catalytic Degradation of Dyes, and Optoelectronic Application. *Crystals* **2023**, *13*, 238. https://doi.org/10.3390/cryst13020238

Academic Editor: Kil Sik Min

Received: 12 January 2023
Revised: 20 January 2023
Accepted: 24 January 2023
Published: 30 January 2023

Copyright: © 2023 by the authors. Licensee MDPI, Basel, Switzerland. This article is an open access article distributed under the terms and conditions of the Creative Commons Attribution (CC BY) license (https://creativecommons.org/licenses/by/4.0/).

1. Introduction

Porphyrins are aromatic tetrapyrrolic macrocycles that are widely represented in living systems. They participate, in a metalated form, in many biological processes. This is the case of hemoglobin and myoglobin, which are built on the basis of the iron protoporphyrin IX complex (heme) and ensure the transport and storage of molecular oxygen [1]. Such natural macromolecules are also involved in the oxidation of substrates by cytochromes (especially cytochromes P450) [2] or in photosynthesis in plants and photosynthetic bacteria.

Unlike iron, cobalt, magnesium, and nickel metals present in natural metalloporphyrins, zinc(II) is not present in biological systems. Nevertheless, synthetic zinc(II) por-

phyrin complexes are actually widely used in a large number of fields, e.g., the manufacture of liquid crystals used in display devices for watches, computer screens, etc. [3,4]. These porphyrinic derivatives are also used in the design of biosensors [5] as well as in photoluminescent [6] and optoelectronic systems [7].

In is worth noting that anion sensing is a rapidly expanding area of research in supramolecular chemistry [8–14]. This stems from many fundamental roles that the anion plays in nature, with biological, chemical, biomedical, and environmental applications.

During the last two decades, many investigations have been devoted to the preparation, characterization, and study of new compounds to be used in the detection of ionic species. Studying the recognition and sensing of such ionic inorganic species is important for several reasons: (i) cationic and anionic inorganic compounds, such as cations of heavy metals (e.g., $Cd^{2+,}$ Hg^{2+}, Pb^{2+}, Sb^{5+}) and many anions (e.g., CN^{-}, $Cr_2O_7^{2-}$, $AsO4^{3-}$), are very toxic and must be removed from the environment; (ii) anions such as NO_3^{-} and PO_4^{2-} are present in agricultural fertilizers; and (iii) many ions, such as K^{+}, Na^{+}, and F^{-}, have very important roles in the functioning of biological systems [15,16]. Among compounds used for the detection and sensing of inorganic ions, metal-organic frameworks (MOFs) should be mentioned in the first place [17,18]. The other important species used as receptors and sensors of anionic and cationic inorganic compounds are the calixarenes, especially the calix [6], homooxacalix [3], and homoazacalix [3] arenes [19,20].

On the other hand, porphyrins and metalloporphyrins are very attractive hosts to use for anion recognition studies, as they are spectrophoto-electroactive, which enables the complexation of anions via several physical methods. It has been shown that the well-known *meso*-tetraphenylporphyrin (H_2TPP) does not have anion binding power alone [21,22]. This is due to the small size of the cavity of this porphyrin, which does not complex anions via hydrogen bonding interactions between the ion anion and the porphyrin N ⋯ H bonds.

In addition, the rigidity of the porphyrin backbone and the cavity also weaken the formation of anionic bonds. This gave rise to the expansion of the porphyrinic cavity. This is the case for urea porphyrins, also known as "picket fence porphyrins" [23], and metalloporphyrin-cage systems [24].

The sensing of anions by hosts that are zinc(II) porphyrin complexes can be monitored by UV-visible spectral titration studies, e.g., the detection of Cl^{-} and Br^{-} ions by the zinc(II) porphyrin complex [24]. On the other hand, recent developments with porphyrin-based solar cells exhibit a promising advance because they use low production cost materials, are easy to synthesize, have low toxicity, rigid geometry, and efficient electron transfer, etc. [25–33]. Moreover, porphyrin-based solar cells possess high molar absorption coefficients and exceptional light harvesting properties, which make them excellent sensitizers for dye-sensitized solar cells (DSSCs) [34–42].

In this work, a new *meso*-porphyrin, namely [4*α*-*meso*-tetra-(1,2,3-triazolyl)-phenylporphyrinato]zinc(II) symbolized by 4α-[Zn(TAzPP)] (**4**), was synthesized using the click chemistry method [43–45], and the ability of this new zinc(II) porphyrin complex to capture Cl^{-} and Br^{-} ions was studied. UV-visible, fluorescence, IR, and ^{1}H NMR spectroscopic characterization of (**4**) is described. The bonding of Cl^{-} and Br^{-} ions by complex (**4**), investigated by UV-visible titration, is also reported. Furthermore, the efficiency of the catalytic oxidative degradation and photocatalysis of rhodamine B (RhB) and methyl orange (MO) dyes using the triazole *meso*-arylporphyrin zinc complex were also investigated. Additionally, the current-voltage characteristics and impedance spectroscopy measurements of 4α-[Zn(TAzPP)] (**4**) were studied to determine their electronic properties.

2. Method and Materials

All commercially available reagents were used without further purification. All anions that were used for selectivity testing were in the form of tetrabutylammonium salt.

UV-visible absorption spectra and titration were recorded on a WinASPECT PLUS (SPECORD PLUS version 4.2 validation) scanning spectrophotometer. ^{1}H NMR spectroscopy was performed on a Bruker DPX 400 spectrometer and chemical shifts are reported

in ppm below the internal tetramethylsilane (TMS) field. IR spectra with Fourier transformation were obtained using a PerkinElmer Spectrum Two FT-IR spectrometer. Emission spectra were recorded in dichloromethane at room temperature on a Horiba Scientific FluoroMax-4 spectrofluorometer. Samples were placed in 1 cm path length quartz cuvettes. Luminescence lifetime measurements were performed after irradiation at = 430 nm obtained by the second harmonic of a titanium: sapphire laser (Tsunami Spectra Physics 3950-M1BB picosecond laser + 39868-03 pulse doubler) at a repetition rate of 800 kHz. The luminescence decays were studied with FLUOFIT software (Picoquant). The emission quantum yields were calculated at room temperature in dichloromethane solutions using the optical dilution method. [Zn(TPP)] in air-equilibrated dichloromethane solution was chosen as the quantum yield standard (ϕ_f = 0.031) [46].

The oxidative degradation and photodegradation of MO and RhB dye experiments were performed at room temperature using 10 mg of the catalyst compound and 10 mL of an aqueous solution of the MO and RhB dyes (at pH = 6). Stirring was kept at 250 rpm. The resulting mixture was filtered, and the concentration was then recorded by measuring the absorption at 555 and 418 nm for MO and RhB dyes, respectively. The decolorization yields (R%) are given by the following relationship (Equation 1):

$$R\% = (A_o - A_t)/A_o.100 \quad (1)$$

where A_o and A_t are the absorption at t = 0 and at the t instant, respectively.

3. Results and Discussion

3.1. Synthesis

4α-*meso*-tetra-*o*-nitrophenylporphyrin($H_2T_{NO2}PP$) was synthesized using the method described in the literature [47]. 4α-*meso*-tetra-*o*-aminophenylporphyrin (**1**) (4α-$H_2T_{NH2}PP$) was then prepared by the reduction of the nitro group of 4α-*meso*-tetra-o-nitrophenylporphyrin to the amine group, following the literature method [47] (Scheme 1). Separation was carried out using a one-column procedure that enriched the desired cis isomer (designated by α atropisomer), as described in the literature [48], leading to 4α-*meso*-tetra-*o*-aminophenylporphyrin (4α-$H_2T_{NH2}PP$) (**1**). 4α-*meso*-tetra-*o*-azidophenylporphyrin (**2**) (4α-$H_2T_{N3}PP$) was produced using sodium nitrite ($NaNO_2$) and sodium azide (NaN_3). Compound (**2**) was then metalated using $Zn(OAc)_2{\cdot}2H_2O$, leading to [4α-meso-tetra(2-azidophenyl)porphyrinate]zinc(II) (**3**) (4α-[$Zn(TN_3PP)$]). Finally, using the click chemistry reaction [49], [4α-*meso*-tetra-(1,2,3-triazolyl)phenylporphyrinato]zinc(II) (**4**) (4α-[Zn(TAzPP)]) was synthesized.

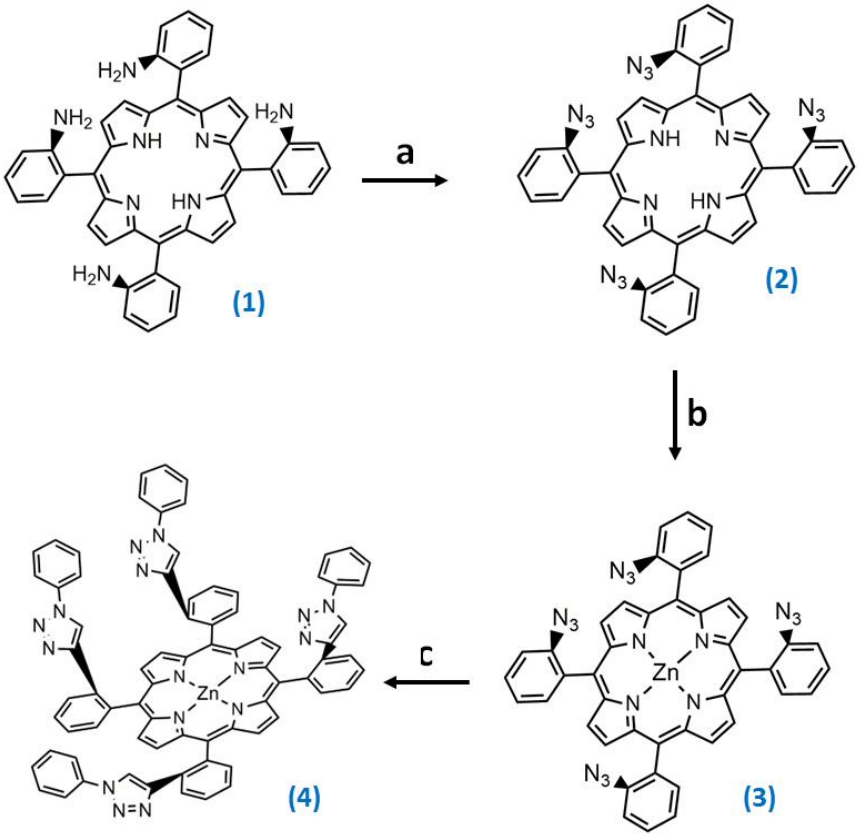
3.2. Spectroscopic ^{1}H NMR and IR Data

For the 4α-$H_2T_{NH2}PP$ (**1**) and 4α-$H_2T_{N3}PP$ (**2**) free-base porphyrins, the characteristic types of protons were observed. Thus, the NH-pyrrolic protons, which are exchangeable and strongly shielded, appeared between −2.5 and −2.7 ppm. The eight β-pyrrolic protons of the porphyrin macrocycle resonated around 8.8 ppm. The phenyl protons of these two *meso*-porphyrins resonated in the range of 8.88 to 7.49 ppm. For the 4α-$H_2T_{NH2}PP$ porphyrin, a singlet was shown around 3.56 ppm, which corresponded to the amine protons (Figures S5 and S6).

The disappearance of the signal at −2.68 ppm, corresponding to NH-pyrrolic protons of compound (**2**), was an indication of the insertion of the Zn(II) ion into the porphyrin ring (Figure S6). The positions of the peaks of the Hβ-pyrrolic protons, as well as those of the phenyl protons of the 4α-[$Zn(TN_3PP)$] and 4α-[Zn(TAzPP)] complexes (**3**)–(**4**), underwent a slight shift compared to those of the 4α-$H_2T_{NH2}PP$ and 4α- $H_2T_{N3}PP$ free-base porphyrins (Figures S5–S8) [49].

The azide stretching vibration ν(N_3) was easily identified from the IR spectra of compounds (**2**) and (**3**), which appeared in the 2130–2068 and 2133–2098 cm^{-1} domains, respectively. The IR spectrum of 4α-[Zn(TAzPP)] (**4**) confirmed the formation of the triazole

meso-arylporphyrin which showed a strong absorption band at 1731 cm^{-1} attributed to the ν(N==N) and ν(C==N) stretching vibrations of the triazole group (Figures S1–S4) [50].



Scheme 1. General scheme for the synthesis of compounds (**1**–**4**): (**a**): (1) HCl, H_2O; (2) $NaNO_2$, HCl, H_2O; (3) NaN_3, HCl, H_2O, (**b**): $Zn(OAc)\cdot 2H_2O$, $CHCl_3/C_2H_5O$, (**c**): CuI, Et_3N, Phenylacetylene, in THF/Acetonitrile.

3.3. Optical Absorption

Figure 1 depicts the electronic absorption spectra of compounds (**1**)–(**4**), while the UV-visible data of these porphyrinic species are given in Table 1. 4α-$H_2T_{NH2}PP$ and 4α-$H_2T_{N3}PP$ free-base *meso*-porphyrins (**1**)–(**2**) presented similar UV-visible spectra in solution, with λ_{max} values of the Soret band at ca. 424 nm and four Q bands at ca. 515, 550, 590, and 660 nm. The UV-visible spectra of the 4α-[Zn($T_{N3}PP$)] (**3**) and 4α-[Zn(TAzPP)] (**4**) Zn(II) porphyrin complexes were slightly shifted compared to those of the corresponding free-base porphyrins, and the number of Q bands was reduced from four to two, which was indicative of the metalation of a porphyrin [51].

The optical gap (E_g-op) values of compounds (**1**)–(**4**) were 1.83, 1.92, 2.02, and 2.03 eV, respectively. In particular, the E_g-op values of Zn(II)-metalloporphyrins were close to 2.00 eV. It is worth mentioning that the optical gap values of the two zinc(II) metalloporphyrins indicated that these complexes could be used for the development of new optoelectronic organic semiconductor materials [52].

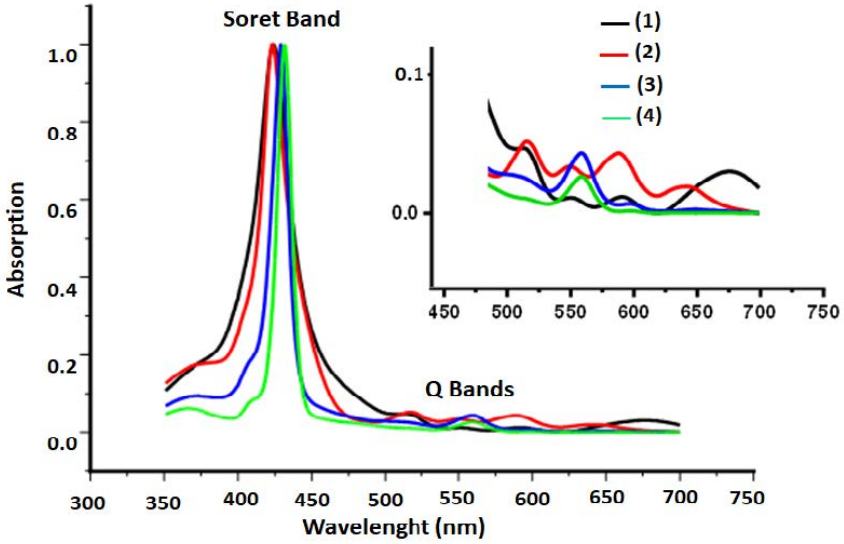


Figure 1. UV–visible spectra of compounds (**1**)–(**4**) recorded in dichloromethane at concentrations ~10^{-6} M. The inset shows the enlarged view of the Q bands region.

Table 1. UV-visible data of the free-base porphyrins and the *meso*-arylporphyrin zinc(II) tetracoordinated complexes. The spectra were recorded in dichloromethane.

	λ_{max} (nm) ($\varepsilon \times 10^{-3}M^{-1}.cm^{-1}$)					$E_{gap\text{-}opt}$ (eV)	Ref
Compound	**Soret band**		***Q* bands**				
Free-base meso-arylporphyrins							
H_2(TPP) [a]	416(419)	513(20)	550(20)	590(6)	646(6)	1.89	[53]
H_2(TEBOP) [b]	422(295)	517(9)	554(8)	593(5)	651(7)	1.85	[54]
H_2(T_{AzP}-IVP) [c]	424(576)	520(46)	555(29)	595(24)	652(18)	1.86	[55]
$H_2T_{NH2}PP$	424(545)	514(39)	552(41)	592(40)	677(35)	1.83	this work
$H_2T_{N3}PP$	424(519)	516(39)	550(37)	594(38)	642(36)	1.92	this work
Zinc(II) meso-arylporphyrin complexes							
[Zn(TPP)]	421(524)	550(21)	591(25)			1.91	[43]
[Zn(T_{AzP}-IVP)]	424(530)	551(26)	592(10)			2.04	[50]
4α-[Zn($T_{N3}PP$)]	430(535)	560(410)	598(361)			2.02	this work
4α-[ZnTAzPP]	430(544)	561(394)	601(321)			2.03	this work

[a]: TTP = *meso*-tetratolylporphyrinato, [b]: TEBOP = *meso*-tetrakis(ethyl-4(4- butyryl)oxyphenyl)porphyrinato, [c]: TAzP-IVP = 4-((1-(4-iodinephenyl)-1H-1,2,3-triazol-4-yl)methoxy)-3-methoxyphenyl.

3.4. Photoluminescence Studies

Porphyrins and metalloporphyrins are known to exhibit two types of emissions. The first emission type, which is between the second excited state S_2 and the ground state S_o ($S_2 \rightarrow S_o$), corresponds to the Q bands [Q (0,0) and Q(0,1)]. The second emission type is between the first exited state S_1 and the ground state S_o ($S_1 \rightarrow S_o$), corresponding to the Soret band. The $S_2 \rightarrow S_o$ emission is very weak and negligeable; only the $S_1 \rightarrow S_o$ emission is considered for porphyrins and metalloporphyrins.

As shown in Figure 2, we noticed a major hypochromic shift of approximately 50 nm of the Q(0,0) and Q(0.1) bands between free-base porphyrins (**1**) and (**2**) and their corresponding zinc porphyrins. The Q(0,0) and Q(0,1) emission bands of compounds (**3**) and (**4**) had wavelengths of about 600 and 665 nm, respectively. The quantum yield values of compounds (**1**)–(**4**) were 0.085, 0.078, 0.054, and 0.033, respectively. The decrease in

the fluorescence quantum yield values (Φ_f) was due to the insertion of zinc(II) on the free-base porphyrins. The fluorescent lifetime values of compounds (**1**)–(**4**) were 8.61, 8.78, 3.1, and 1.91, respectively. The photophysical property values of the synthesized compounds showed that they could be used for various optoelectronic applications, a priori DSSC systems.

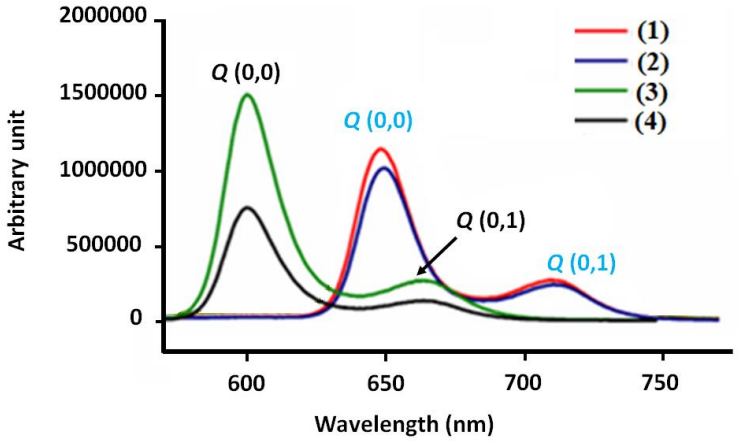


Figure 2. Emission spectra of compounds (**1**)–(**4**). The spectra were recorded in dichloromethane at concentrations ~10^{-6} M. The excitation wavelength value was 430 nm.

3.5. Anion Binding Studies

[4α-*meso*-tetra-(1,2,3-triazolyl)phenylporphyrinato]zinc(II) complex (**4**) (4α-[Zn(TAzPP)]) was tested as a detector of Cl^- and Br^- anions by UV-visible titration in dichloromethane. Anions were added as their salts of the non-complexing cation tetrabutylammonium (TBA).

The UV-visible titration spectra of complex (**4**) showed a clear change of the Soret and Q bands as the concentration of the Cl^- and Br- anions increased (Figure 3a,b). The titrations for Cl^- and Br^- ions on [Zn(TTP)] (TTP = *meso*-tolylporphyrin) used as a reference are shown in Figure 3c,d. Table 2 summarizes the values of the association constants K_{as} for [Zn(Porph)Cl] (Porph = TTP and TAzPP) and [Zn(Porph)Br] complexes. The K_{as} values obtained from the titration of the [Zn(PC)X] complex with the cage porphyrin (PC = 4α-*meso*-(tetrakis(2-azidoacetamidophenyl)porphyrinate [23] with Cl^- and Br^- ions are also shown in Table 2.

Upon successive addition of Cl^- to complex (**4**), the UV-visible titration study showed a bathochromic shift of the Soret band from 430 to 439 nm ($\Delta\lambda_{max}$ = 9 nm), with one distinct isosbestic point at 434 nm, thus proving the formation of a 1:1 coordination complex type [Zn(Porph)(L)] (L = axial ligand). A red shift was also observed for the Q(0,0) and Q(0,1) bands. Similar changes were also noted upon Br^- addition to a solution of 4α-[Zn(TAzPP)] (**4**), using the same concentrations, showing a red shift of the Soret and Q bands. As the titration progressed, an isosbestic point was also observed at 436 nm for the Soret band.

A UV-visible titration with zinc(II)-*meso*-tetratolylphenylporphyrin ([Zn(TTP)]) was also performed to compare the Cl^- and Br^- detecting properties of zinc complex (**5**) with those of the [Zn(TTP)] complex.

The association constants for the 1:1 complex, calculated using the so-called "strong interactions" method [56] (see the supplementary information for details), are summarized in Table 2. From this table, it can be seen that in the case of Cl-, the average K_{as} value of 4α-[Zn(TAzPP)] (**4**) was 0.301 × 10^3, which was higher than that of [Zn(TTP)] porphyrin with a K_{as} value equal to 0.063 × 10^3. On the other hand, these two values were far lower than that obtained with the cage porphyrin PC [23], with a value is equal to 1.220 × 10^4. For the bromide ion, the K_{as} values were 0.441 × 10^3 for porphyrin derivative (**4**) and 0.168 × 10^3 for the [Zn(TTP)] complex, while the association constant K_{as} value for [Zn(PC)Br] was equal to 0.005 [23]. These results showed that our synthetic zinc(II) porphyrin 4α-[Zn(TAzPP)] (**4**) was selective for Br− over Cl^- anions and that complex (**4**) presented a

better binding affinity for Br^- than the cage porphyrin (PC). This could be explained by the fact that the cage porphyrin has a cavity which is not large enough to accommodate the large size of the bromide ion.

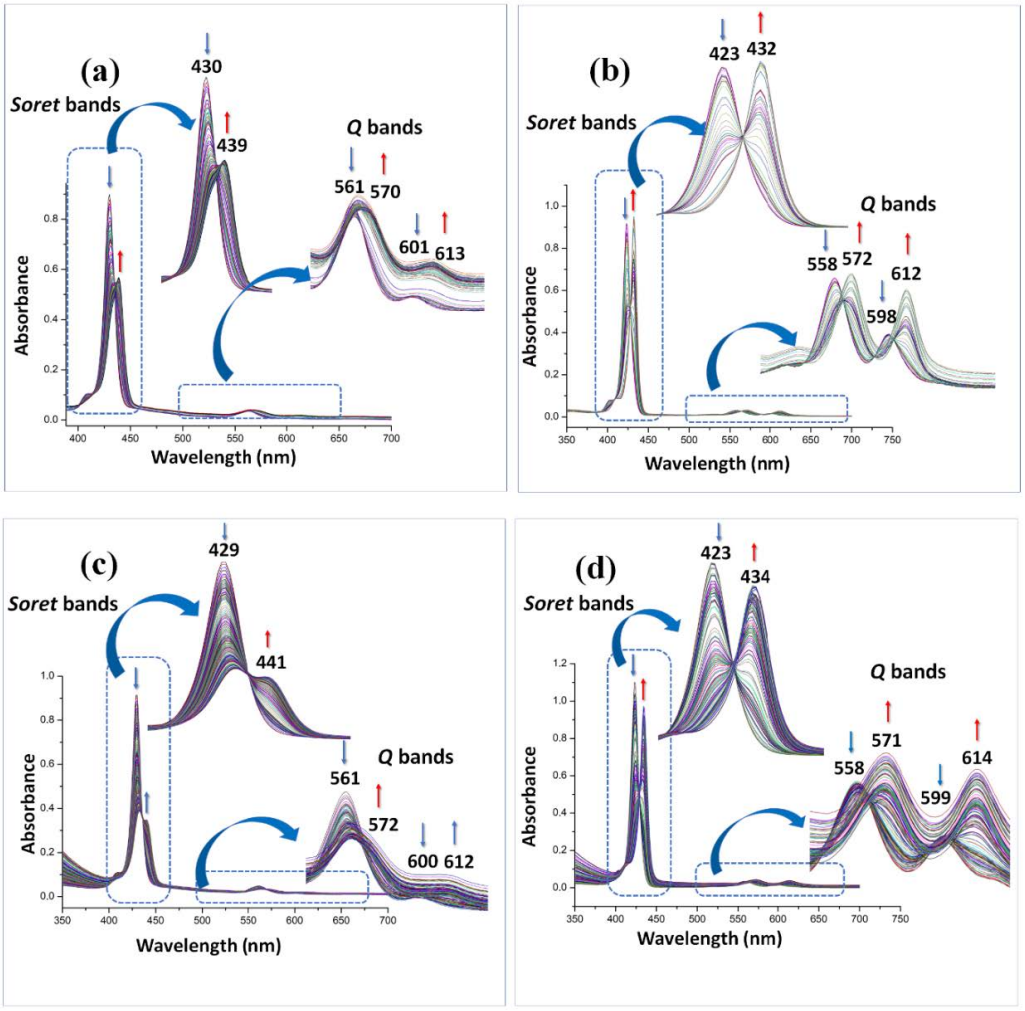


Figure 3. Evolution of the Q and Soret bands: (**a**) complex (**4**) as a function of the addition of the Cl^- anion, (**b**) [Zn(TTP)] as a function of the addition of the Cl^- anion, (**c**) complex (**4**) as a function of the addition of the Br^- anion, and (**d**) [Zn(TTP)] as a function of the addition of the Br^- anion.

Table 2. Values of association constants (K_{as}) and log(K_{as}) for our zinc(II) metalloporphyrins and other related complexes.

Complexes	log(K_{as})	(K_{as})	Ref.
[Zn(TAzPP)Cl]	2.407	0.301×10^3	this work
[Zn(TTP)Cl]	1.791	0.063×10^3	this work
[Zn(PC)Cl]	-	1.220×10^4	[23]
[Zn(TAzPP)Br]	1.299	0.441×10^3	this work
[Zn(TTP)Br]	1.789	0.168×10^3	this work
[Zn(PC)Br]	-	0.005	[23]

3.6. Degradation of Rhodamine B (RhB) and Methyl Orange (MO) Dyes

The ability of complex (**4**) to catalyze the degradation of RhB and MO dyes was tested using an aqueous hydrogen peroxide solution at room temperature. The optimal condition

of this degradation was found to be as follows: mass of complex (**4**) was m = 10 mg, the H_2O_2 aqueous solution concentration was C_o = 20 mg.L^{-1}.

The oxidation of organic compounds by hydrogen peroxide catalyzed per metallic species is known to involve the radical •OH, leading to a formation of intermediate species. In our case, the disappearance rate of the RhB and MO dyes could be obtained through the following equation (Equation (2)):

$$\frac{dC}{dt} = -k.C.[OH^{\cdot}] \quad (2)$$

where C is the concentration of the MO and RhB dyes at time t and k is defined as the second order rate constant of the MO and Rh B dyes reacting with •OH. The equation can be further simplified if one considers that the concentration of •OH is constant, assuming the steady state situation for the net formation rate of these intermediates. Thus, the degradation rate of the MO and RhB dyes due to the combination of hydrogen peroxide is finally given by Equation (3):

$$\frac{dC}{dt} = -k_o.C \quad (3)$$

where k_o (in min^{-1}) is the pseudo-first order rate constant, and C_t and C_o are the concentrations at time t and the initial concentration, respectively. Figure 4 shows the curves C_t/C_o versus time. The degradation yield (R%) is given by the following relation (Equation (4)):

$$R(\%) = \left(\frac{C_o - C_t}{C_o}\right).100 \quad (4)$$

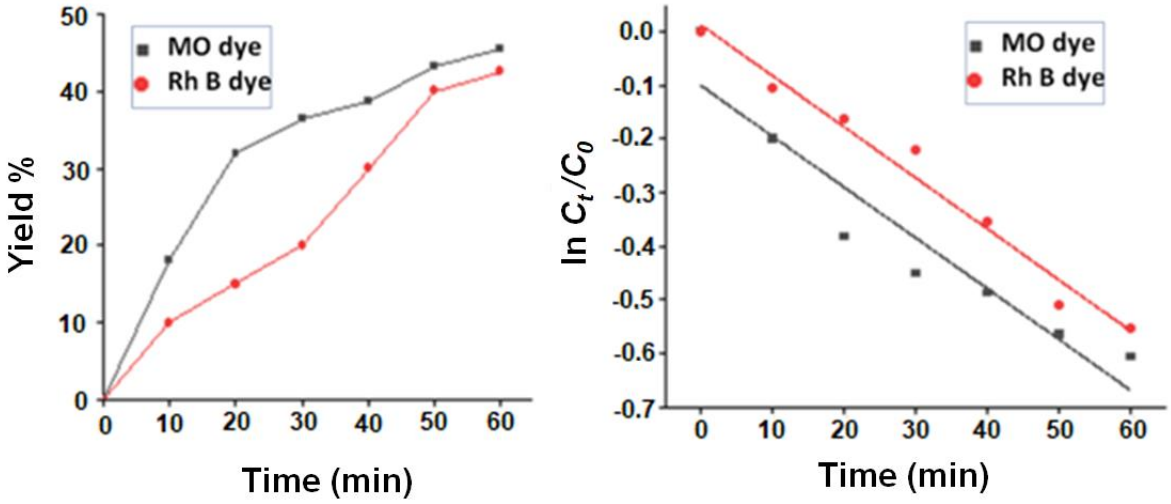


Figure 4. (Left) Changes in C_t/C_o versus time for the following conditions: H_2O_2 + MO + complex (**4**) and H_2O_2 + Rh B + complex (**4**). (Right) Kinetics of complex (**4**)-catalyzed degradation of MO and Rh B in aqueous solution.

As shown in Figure 4, when we used only MO and Rh B dyes with the H_2O_2 aqueous solution, there was no degradation of the organic dyes. The use of an aqueous solution of H_2O_2 (C_o = 10 mg.L^{-1}) led to degradation yields of 45.5% and 42.3% for the MO and RhB dyes, respectively, after 60 min of reaction. The k_o values of the pseudo-first order rate constant of the degradation concerning the MO or RhB dye-H_2O_2-complex (**4**) systems were 0.01 × 10^{-2} min^{-1} (R^2 = 0.9017) and 0.011 × 10^{-2} min^{-1} (R^2 = 0.9776), respectively.

3.7. Photodegradation of MO and RhB Dyes

First, complex (**4**) was utilized to degrade MO and RhB dyes under visible light illumination (λ > 400 nm) for the sake of exploring further photocatalytic transformations.

In a typical trial, an aqueous suspension (50 mL) containing MO or RhB dye (20 mg/L) and 10 mg of complex (**4**) was placed in the reactor under visible light irradiation. The suspension was stirred in the dark for 30 min before illumination to ensure the adsorption/desorption balance was established.

At defined time intervals, an appropriate amount of suspension was centrifuged and filtered through a filter membrane to remove solid particles and collect the filtrate for further analysis. The maximum absorption wavelength of the MO and RhB dyes (λ_{max}) were 418 and 555 nm, respectively.

As shown in Figure 5, complex (**4**) showed effective degradation of MO dye. More than 75% of the RhB dye was degraded after irradiation for 60 min, while the percentage of degradation of the MO dye was 63%.

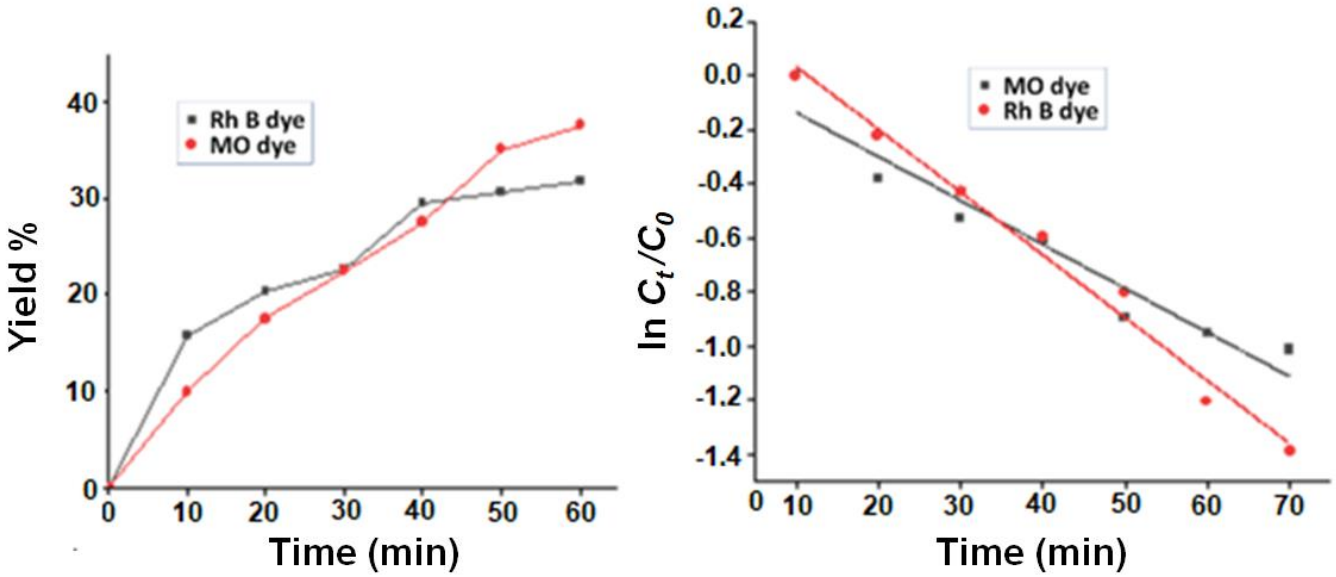


Figure 5. (**Left**) Changes in C_t/C_o versus time for the following conditions: MO + complex (**4**) and RhB + complex (**4**). (**Right**) Kinetics of complex (**4**)-catalyzed photo degradation of MO and Rh B dyes in aqueous solution.

The kinetics of the degradation reaction can be described using a first-order model for low concentrations of the MO and RhB dye solutions. The pseudo first-order kinetics equation is expressed as follows (Equation (5)):

$$\ln(C_o/C_t) = k_o t \quad (5)$$

where C_t is the MO or Rh B dye concentration in aqueous solution at time t (mg/L), C_o is the initial MO or RhB dye concentration (mg/L), and k_o is the apparent pseudo-first-order kinetic constant (min^{-1}). The plots $\ln(C_t/C_o)$ as a function of time are shown in Figure 5. The calculated values of k_o were 1.6×10^{-2} min^{-1} (R^2 = 0.9344) and 2.3×10^{-2} min^{-1} (R^2 = 0.9856) for the MO and RhB dyes, respectively. The excellent fitting indicated that the photoreaction followed first-order reaction kinetics.

The principle of heterogeneous photocatalysis (Figure 6) is based on the activation of complex (**4**) by a supply of light energy hν ≥ Eg (Eg = band gap energy). During this activation step, an electron (e−)/hole (h+) pair is created, which results from the passage of an electron from the valence band to the conduction band. The electron will react with the oxygen adsorbed on the surface of our porphyrinic compounds, while the hole h+, reacts with the surface of the OH ions to form highly oxidizing hydroxyl radicals (OH·), which is responsible for the degradation of pollutants.

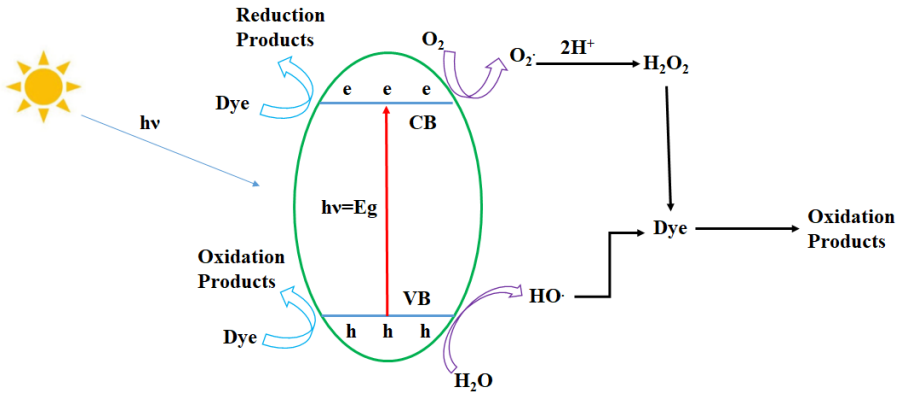


Figure 6. Pictorial representation of indirect dye degradation process.

Complex (**4**), repeatedly used, exhibited properties identical to those of the initial complex, with no obvious drop in photocatalytic efficacy even after five cycles, achieving photodegradation efficiency of 60% and 73% for the MO and RhB dyes, respectively (Figure 7).

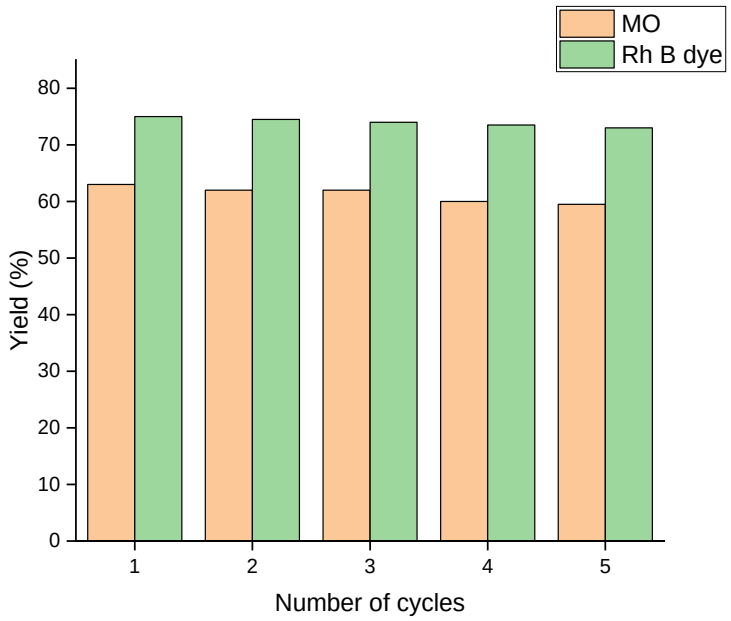


Figure 7. Redegradation efficiency of complex (**4**) for the MO and RhB dyes.

4. Electronic Study on Complex (4)

To prepare the thin film containing complex (**4**), ITO glass slides were washed in an ultrasonic bath containing acetone, then in an isopropyl alcohol bath. Subsequently, the clean substrates were dried with a nitrogen gas flow. A 15 mg sample of complex (**4**) was dissolved in 10 mL of dichloromethane. Afterwards, the solution containing the zin(II) coordination compound was deposited on an indium tin oxide (ITO) glass slides by spin coating at 2000 rpm for 25 s. The aluminum (Al) electrodes were deposited by thermal evaporation. To obtain the best quality images of the film surface, AFM (atomic force microscopy) was employed, which showed the homogeneity of the film with a coherent structure (1.86 nm).

Owing to the interesting value of the gap energy of complex (**4**), which was in the range of semiconductor materials, we carried out electrical and dielectric tests on this new zinc(II) porphyrin compound in order to study its electronic properties.

The I-V measurements were obtained using a Keithley 236 instrument and the spectroscopic impedance measurement was performed using an impedance analyzer (Solartron 1260). The electronic properties of the ITO/complex (**4**)/Al system can provide information about the transmission properties in organic materials. The current-voltage curve measured at room temperature of the ITO/Complex (**4**)/Al system is shown in Figure 8. The curve shown in this figure presents a similar behavior to that of electronic devices, such as diodes, indicating complex (**4**) could be used as a photosensitizer in DSSCs (dye-sensitized solar cells) [57–60]. The threshold voltage was approximately 0.64 V.

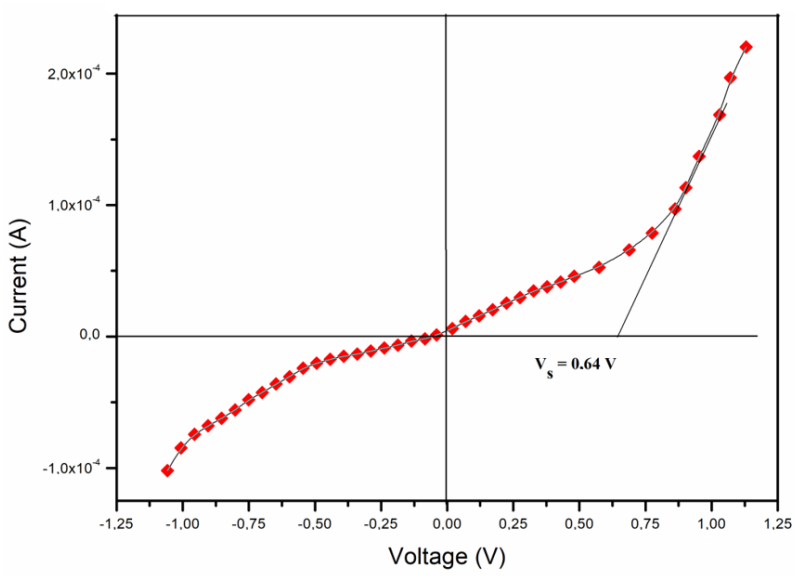


Figure 8. Current–voltage curves of ITO/complex (**4**).

Indeed, we observed an asymmetric curve for high voltage, which was related to the difference in the injection of electrons and holes of the anode (ITO) and cathode (Al). At low voltage, the I-V curve indicated symmetric behavior. This behavior is explained by the theory that the localized state with defects provides the localized gap states.

Notably, recent work [61] has shown a useful current hysteresis behavior for some porphyrin species. By introducing a triazole group, the hysteresis behavior was eliminated and consequently, we completely changed the electronic properties of our tested molecule.

The semi-logarithmic scale of the I-V curve of complex (**4**) indicated that the value of the barrier height of this species was approximately 1.3083 V and the saturation current value was 5.97×10^{-6} A.

In addition, we studied the mechanism of electrical conduction through the junction by presenting the I-V characteristics in double logarithmic plot (Figure 9). The I-V plot of the ITO/complex (**4**)/Al system showed the presence of different parts in which the current depended mainly on the applied voltage. At low voltage, the first part of the curve corresponded to a value of the slope in the order of 1.2, indicating prevention of the charge injection due to the presence of a small amount of interface barrier. For this part of the curve, which defines the ohmic region, the amount of the heat-activated charge carriers was too small and the trap levels were vacant. The current density equation is as follows (Equation (6)):

$$J_\Omega = q.p_0.\mu.\frac{V}{d} \quad (6)$$

where μ represent the charge mobility, q defines the electronic charge, d refers to the film thickness, and p_0 is the free carrier density.

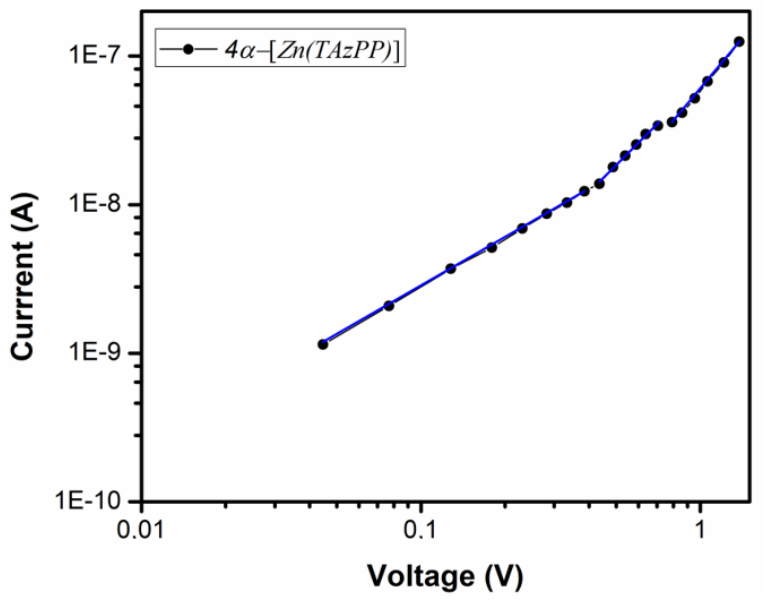


Figure 9. Log-log curve of complex (**4**) structure.

In the second part of the curve, where the voltage was moderate, the value of the slope was close to 2.2. This can be explained by the dependence of the voltage according to the power law (I-V), which is associated with the space charge limited current mechanism (SCLC) [62]. In addition, the applied voltage increased and passed through the transition voltage, which reflected the increase in the density of charges injected by the electrodes. The charge density injected will govern the transport ability of the layer of complex (**4**). The current density varies following equation (Equation (7)):

$$J_{SCLC} = \frac{9}{8}\varepsilon.\mu_{eff}.\frac{V^2}{d^3} \quad (7)$$

where d is the film thickness, V is the applied voltage, ε is the material permittivity, and μ_{eff} is the effective carrier mobility.

Based on the SCLC model (Equation (7)), the μ_{eff} in the film of complex (**4**) had a value of 0.45 (10^{-5} cm^2/Vs). In the third part of the curve, where the voltage is high, the value of the slope was approximately 3.4. This represented the trapped charge limit current (TCLC) area where the distribution of traps changed exponentially. However, the transition between SCLC and TCLC mechanisms is affected by the trapping levels. This transition occurs when the quantity of injected carriers surpasses the density of free carriers [63].

4.1. Impedance Spectroscopy

To investigate the dielectric characteristics of complex (**4**) and determine the participation associated with the volume and interface, we carried out an impedance spectroscopy study [64–66]. Equation (**8**) describes the impedance Z(ω) of complex (**4**) as a function of frequency:

$$Z(\omega) = \text{Re}\ (Z) + j\text{Im}\ (Z) = Z'(\omega) + jZ''(\omega) \quad (8)$$

This equation shows that the complex impedance Z(ω) is composed of two parts: the first part is the real part (Re (Z) = Z′) and the second part is the imaginary part (Im (Z) = Z″). The semicircular spectrum present in the impedance spectrum (Nyquist plot) of the complex (**4**) structure suggested the homogeneity of the electrode-organic interface (Figure 10).

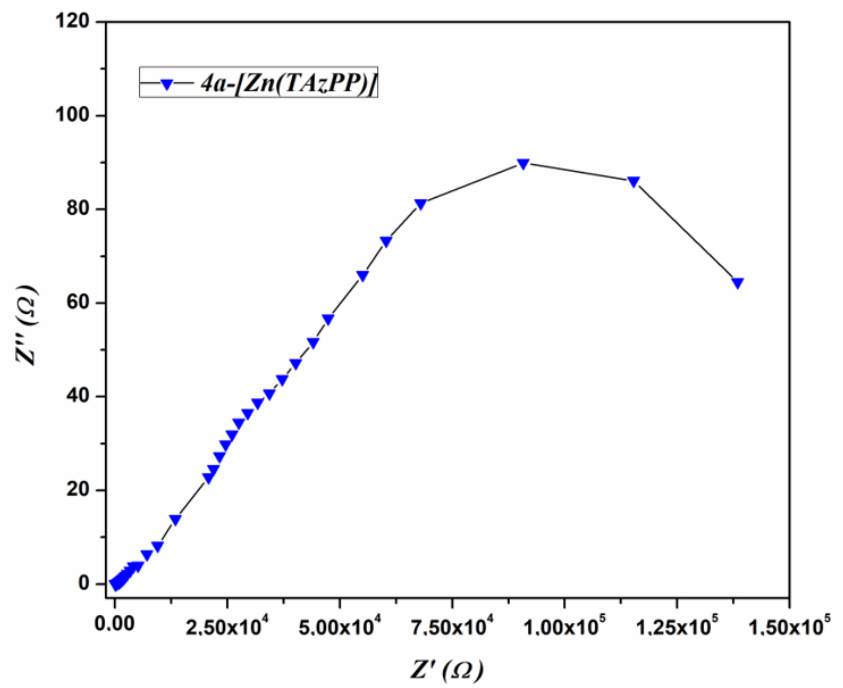


Figure 10. Impedance plot spectrum of complex (**4**).

4.2. Conductance

Figure 11 shows two regimes of conductance of complex (**4**), which depended essentially on the frequency applied. The first regime was observed at low frequency, where the conductance increased with increasing frequency until reaching a maximum at a frequency of approximately 1.4 Hz, which indicated a disordered system. However, the second regime observed at high frequency indicated that the conductance tended toward zero, where the dipoles neglected the frequency. This phenomenon was associated with the jump transport mechanism, where the dipoles will be guided by the applied field, which will lead to an increase in the charge hopping process (Figure 11) [67].

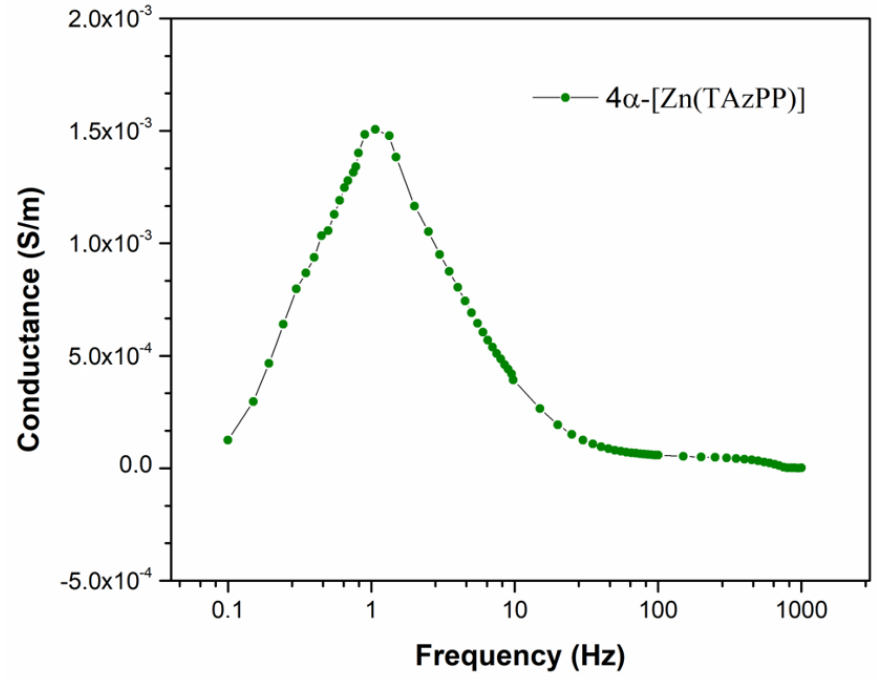


Figure 11. Conductance characteristics of complex (**4**).

5. Conclusions

We successfully synthesized a new zinc(II) *meso*-arylporphyrin coordination compound: [*meso*-4α-tetra-(1,2,3-triazolyl)phenylporphyrinato]zinc(II) (**4**) with the formula 4α-[Zn(TAzPP)]. This new Zn(II) metalloporphyrin was characterized by ^{1}H NMR and infrared, UV-visible, and fluorescence spectroscopies. This coordination compound was able to make 1:1 stoichiometric complexes with Cl^- and Br^- ions, with average association constant values of 0.30×10^3 and 0.44×10^3, respectively, which were higher than those of the related [Zn(TPP)] (TPP = *meso*-tetraphenylporphyrinate) complex. In addition, complex (**4**) was tested as a catalyst in the degradation reaction of rhodamine B (RhB) and methyl orange (MO) dyes, using both photodegradation and degradation by aqueous hydrogen peroxide solution. The photodegradation yield values of the MO and RhB dyes using complex (**4**) were close to 63% and 75%, respectively, while the degradation yield values using aqueous dye solutions, H_2O_2, and complex (**4**) were 45.5% and 42.3% for MO and RhB, respectively. Notably, the use of this complex several times without variation in the degradation yield of the MO and RhB dyes indicated that complex (**4**) was a good catalyst for such reactions. Furthermore, our new Zn(II)-porphyrin species was used in the ITO/complex (4)/Al system for current-voltage and impedance spectroscopy measurements. The I-V curve of this system exhibited a similar behavior to that of diodes, with a threshold voltage of approximately 0.64 V. The impedance spectrum (Nyquist plot) of complex (**4**) presented a semicircular spectrum that suggested the homogeneity of the electrode-organic interface. Finally, the conductance properties of complex (**4**) were investigated, indicating the presence of two regimes of conductance depending essentially on the frequency applied.

Supplementary Materials: The following supporting information can be downloaded at: https://www.mdpi.com/article/10.3390/cryst13020238/s1, Figure S1: IR spectrum of the free base porphyrin (4α-H_2TNH_2PP) (**1**); Figure S2: IR spectra of the free base porphyrin 4α-H_2TN_3PP (**2**); Figure S3: IR spectra of the complex 4α-[Zn(TN_3PP)]) (**3**); Figure S4: IR spectra of complex 4α-[Zn(TAzPP)] (**4**); Figure S5: ^{1}H NMR spectrum of the free base porphyrin 4α-H2TNH2PP (**1**) (400 MHz, $CDCl_3$); Figure S6: ^{1}H NMR spectrum of free base porphyrin 4α-H2TN3PP (**2**) (400 MHz, $CDCl_3$); Figure S7: ^{1}H NMR spectrum of 4α-[Zn(TN_3PP)] (**3**) (400 MHz, $CDCl_3$); Figure S8: ^{1}H NMR spectrum of α4-[Zn(TAZPP)] compound (**4**) (400 MHz, $CDCl_3$).

Author Contributions: Conceptualization, S.N., M.G., J.B., Y.O.A.-G. and H.N.; Methodology, J.B. and F.L.; Software, Y.O.A.-G. and F.L.; Validation, J.B. and H.N.; Formal analysis, F.L.; Investigation, M.G. and F.L.; Writing–original draft, S.N., M.G. and J.B.; Writing–review & editing, H.N.; Visualization, H.N.; Project administration, S.N., J.B and Y.O.A.-G. All authors have read and agreed to the published version of the manuscript.

Funding: The authors extend their appreciation to the deputyship for Research & Innovation, Ministry of Education in Saudi Arabia for funding this research work through the project number (IFP-2020-05).

Data Availability Statement: Not applicable.

Conflicts of Interest: The authors declare no conflict of interest.

References

1. Perutz, M. Regulation of Oxygen Affinity of Hemoglobin: Influence of Structure of the Globin on the Heme Iron. *Ann. Rev. Biochem.* **1979**, *48*, 327. [CrossRef] [PubMed]
2. Milgrom, L.R. *The Colors of Life: An Introduction to the Chemistry of Porphyrins and Related Compounds*; Oxford University Press: New York, NY, USA, 1997; p. 249.
3. Campbell, W.M.; Jolley, K.W.; Wagner, P.; Wagner, K.; Walsh, P.J.; Gordon, K.C.; Schmidt-Mende, L.; Nazeeruddin, M.K.; Wang, Q.; Grätzel, M.; et al. Highly Efficient Porphyrin Sensitizers for Dye-Sensitized Solar Cells. *J. Phys. Chem. C. Lett.* **2007**, *111*, 11760. [CrossRef]
4. Gregg, B.A.; Fox, M.A.; Bard, A.J. Functionalized Porphyrin Discotic Liquid Crystals. *J. Am. Chem. Soc.* **1989**, *111*, 3024. [CrossRef]
5. Garg, K.; Singh, A.; Majumder, C.; Nayak, S.K.; Aswal, D.K.; Gupta, S.K.; Chattopadhyay, S. Room temperature ammonia sensor based on jaw like bis-porphyrin molecules. *Org. Electron.* **2013**, *14*, 14189. [CrossRef]

6. Kadish, K.M.; Smith, K.M.; Guilard, R.; Harvey, P.D. *The Porphyrin Handbook*; Academic Press: San Diego, CA, USA, 2003; Volume 18, p. 63.
7. Lammi, R.K.; Ambroise, A.; Balasubramanian, T.; Wagner, R.W.; Bocian, D.F.; Holten, D.; Lindsey, J.S. One-step synthesis and characterization of difunctionalized N-confused tetraphenylporphyrins. *J. Am. Chem. Soc.* **2000**, *122*, 7579. [CrossRef]
8. Izatt, R.M.; Pawlak, K.; Bradshaw, J.S. Thermodynamic and kinetic data for macrocycle interaction with cations, anions, and neutral molecules. *Chem. Rev.* **1995**, *95*, 2529. [CrossRef]
9. Dietrich, B. Design of anion receptors: Applications. *Pure Appl. Chem.* **1993**, *65*, 1457. [CrossRef]
10. Kavallieratos, K.; de Gala, S.R.; Austin, D.J.; Crabtree, R. A readily available non-preorganized neutral acyclic halide receptor with an unusual nonplanar binding conformation. *J. Am. Chem. Soc.* **1997**, *119*, 2325. [CrossRef]
11. Davis, A.P.; Perry, J.J.; Williams, R.P. Anion recognition by tripodal receptors derived from cholic acid. *J. Am. Chem. Soc.* **1997**, *119*, 1793. [CrossRef]
12. Berger, M.; Schmidtchen, F. Electroneutral artificial hosts for oxoanions active in strong donor solvents. *J. Am. Chem. Soc.* **1996**, *118*, 8947. [CrossRef]
13. Kral, V.; Furuta, H.; Shreder, K.; Lynch, V.; Sessler, J.L. Protonated sapphyrins. Highly effective phosphate receptors. *J. Am. Chem. Soc.* **1996**, *118*, 1595. [CrossRef]
14. Gale, P.A.; Sessler, J.L.; Kral, V.; Lynch, V. Calix [4] pyrroles: Old yet new anion-binding agents. *J. Am. Chem. Soc.* **1996**, *118*, 5140. [CrossRef]
15. Andrews, P.A.; Mann, S.C.; Huynh, H.H.; Albright, K.D. Role of the Na+,K+-Adenosine Triphosphatase in the Accumulation of cis-Diamminedichloroplatinum(II) in Human Ovarian Carcinoma Cells. *Cancer Res.* **1991**, *51*, 3677.
16. Zhou, Y.; Dong, X.; Zhang, Y.; Tong, P.; Qu, J. Highly selective fluorescence sensors for the fluoride anion based on carboxylate-bridged diiron complexes. *Dalton Trans.* **2016**, *45*, 6839. [CrossRef] [PubMed]
17. Mandal, T.N.; Karmakar, A.; Sharma, S.; Ghosh, S.K. Metal-Organic Frameworks (MOFs) as Functional Supramolecular Architectures for Anion Recognition and Sensing. *Chem. Rec.* **2018**, *18*, 154. [CrossRef] [PubMed]
18. Rozveh, Z.S.; Kazemi, S.; Karimi, M.; Ali, G.A.; Safarifard, V. Photocatalytic aerobic oxidative functionalization (PAOF) reaction of benzyl alcohols by GO-MIL-100(Fe) composite in glycerol/K2CO3 deep eutectic solvent. *Polyhedron* **2020**, *183*, 113514.
19. Dieleman, C.B.; Matt, D.; Neda, I.; Schmutzler, R.; Harriman, A.; Yaftian, R. Hexahomotrioxacalix [3] arene: A scaffold for a C 3-symmetric phosphine ligand that traps a hydrido-rhodium fragment inside a molecular funnel. *Chem. Commun.* **1999**, 1911. [CrossRef]
20. Kumar, R.; Sharma, A.; Singh, H.; Suating, P.; Kim, H.S.; Sunwoo, K.; Shim, I.; Gibb, B.C.; Kim, J.S. Hexahomotrioxacalix [3] arene: A scaffold for a C 3-symmetric phosphine ligand that traps a hydrido-rhodium fragment inside a molecular funnel. *Chem. Rev.* **2019**, *119*, 9657. [CrossRef] [PubMed]
21. Sessler, J.L.; Cyr, M.; Furuta, H.; Kral, V.; Mody, T.; Morishima, T.; Shionoya, M.; Weghorn, S. Anion binding: A new direction in porphyrin-related research. *Pure. Appl. Chem.* **1993**, *65*, 393. [CrossRef]
22. Sessler, J.L.; Burrell, A.K. Sapphyrins and heterosapphyrins. *Top. Curr. Chem.* **1992**, *161*, 177. [CrossRef]
23. Shionoya, M.; Furuta, H.; Harriman, A.; Sessler, J.L. Diprotonated sapphyrin: A fluoride selective halide anion receptor. *J. Am. Chem. Soc.* **1992**, *114*, 5714. [CrossRef]
24. Gilday, L.C.; White, N.G.; Beer, D. Halogen-and hydrogen-bonding triazole-functionalised porphyrin-based receptors for anion recognition. *Dalton Trans.* **2013**, *42*, 15766. [CrossRef] [PubMed]
25. Imahori, H.; Umeyama, T.; Ito, S. Large π-aromatic molecules as potential sensitizers for highly efficient dye-sensitized solar cells. *Acc. Chem. Res.* **2009**, *42*, 1809. [CrossRef] [PubMed]
26. Radivojevic, I.; Varotto, A.; Farley, C.; Drain, C.M. Commercially viable porphyrinoid dyes for solar cells. *Energy. Environ. Sci.* **2010**, *3*, 1897. [CrossRef]
27. Martinez-Diaz, M.V.; Torre, G.; Torres, T. Lighting porphyrins and phthalocyanines for molecular photovoltaics. *Chem. Commun.* **2010**, *46*, 7090. [CrossRef]
28. Walter, M.G.; Rudine, A.B.; Wamser, C.C. Porphyrins and phthalocyanines in solar photovoltaic cells. *J. Porph. Phthalocyanines* **2010**, *14*, 759. [CrossRef]
29. Griffith, M.J.; Sunahara, K.; Wagner, P.; Wagner, K.; Wallace, G.G.; Officer, D.L.; Furube, A.; Katoh, R.; Mori, S.; Mozer, A.J. Porphyrins for dye-sensitised solar cells: New insights into efficiency-determining electron transfer steps. *Chem. Commun.* **2012**, *48*, 4145. [CrossRef] [PubMed]
30. Imahori, H.; Umeyama, T.; Kurotobi, K.; Takano, Y. Self-assembling porphyrins and phthalocyanines for photoinduced charge separation and charge transport. *Chem. Commun.* **2012**, *48*, 4032. [CrossRef]
31. MPanda, K.; Ladomenou, K.; Coutsolelos, A.G. Porphyrins in bio-inspired transformations: Light-harvesting to solar cell. *Coord. Chem. Rev.* **2012**, *256*, 2601.
32. Hasobe, T.; Imahori, H.; Kamat, P.V.; Ahn, T.K.; Kim, S.K.; Kim, D.; Fujimoto, A.; Hirakawa, T.; Fukuzumi, S. Photovoltaic cells using composite nanoclusters of porphyrins and fullerenes with gold nanoparticles. *J. Am. Chem. Soc.* **2005**, *127*, 1216. [CrossRef]
33. Yella, A.; Lee, H.W.; Tsao, H.N.; Yi, C.; Chandiran, A.K.; Nazeeruddin, M.K.; Diau, E.W.; Yeh, C.Y.; Zakeeruddin, S.M.; Grätzel, M. Porphyrin-sensitized solar cells with cobalt (II/III)–based redox electrolyte exceed 12 percent efficiency. *Science* **2011**, *334*, 629. [CrossRef] [PubMed]

34. Kay, A.; Grätzel, M. Artificial photosynthesis. 1. Photosensitization of titania solar cells with chlorophyll derivatives and related natural porphyrins. *J. Phys. Chem.* **1993**, *97*, 6272. [CrossRef]
35. Cherian, S.; Wamser, C.C. Adsorption and Photoactivity of Tetra(4-carboxyphenyl)porphyrin (TCPP) on Nanoparticulate TiO_2. *J. Phys. Chem. B.* **2000**, *104*, 3624. [CrossRef]
36. Nazeeruddin, M.K.; Humphry-Baker, R.; Officer, D.L.; Campbell, W.M.; Burrell, A.K.; Grätzel, M. Conformation and π-conjugation of olefin-bridged acceptor on the pyrrole β-carbon of nickel tetraphenylporphyrins: Implicit evidence from linear and nonlinear optical properties. *Langmuir* **2004**, *20*, 6514. [CrossRef]
37. Wang, Q.; Campbell, W.M.; Bonfantani, E.E.; Jolley, K.W.; Officer, D.L.; Walsh, P.J.; Gordon, K.; Humphry-Baker, R.; Nazeeruddin, M.K.; Grätzel, M. Efficient Light Harvesting by Using Green Zn-Porphyrin-Sensitized Nanocrystalline TiO2 Films. *J. Phys. Chem. B.* **2005**, *109*, 15397. [CrossRef]
38. Park, J.K.; Lee, H.R.; Chen, J.; Shinokubo, H.; Osuka, A.; Kim, D. Photoelectrochemical Properties of Doubly β-Functionalized Porphyrin Sensitizers for Dye-Sensitized Nanocrystalline-TiO2 Solar Cells. *J. Phys. Chem. C* **2008**, *112*, 16691. [CrossRef]
39. Bessho, T.; Zakeeruddin, S.M.; Yeh, C.Y.; Diau, E.W.G.; Grätzel, M. Highly efficient mesoscopic dye-sensitized solar cells based on donor–acceptor-substituted porphyrins. *Angew.Chem. Int. Ed.* **2010**, *49*, 6646. [CrossRef]
40. Campbell, W.M.; Burrell, A.K.; Officer, D.L.; Jolley, K.W. Efficient Light Harvesting by Using Green Zn-Porphyrin-Sensitized Nanocrystalline TiO2 Films. *Coord. Chem. Rev.* **2004**, *248*, 1363. [CrossRef]
41. He, H.; Gurung, A.; Si, L. 8-Hydroxylquinoline as a strong alternative anchoring group for porphyrin-sensitized solar cells. *Chem. Commun.* **2012**, *48*, 5910. [CrossRef]
42. Kolb, H.C.; Finn, M.G.; Sharpless, K.B. Click chemistry connections for functional discovery. *Angew. Chem. Int. Ed.* **2001**, *40*, 2004. [CrossRef]
43. Rostovtsev, V.V.; Green, L.G.; Fokin, V.V.; Sharpless, K.B. A Stepwise Huisgen Cycloaddition Process: Copper(I)-Catalyzed Regioselective "Ligation" of Azides and Terminal Alkynes. *Angew. Chem. Int. Ed.* **2002**, *41*, 2596. [CrossRef]
44. Shetti, V.S.; Ravikanth, M. Synthesis and studies of Thiacorroles. *Eur. J. Org. Chem.* **2010**, *75*, 4172–4182. [CrossRef] [PubMed]
45. Chatterjee, S.; Sengupta, K.; Bhattacharyya, S.; Nandi, A.; Samanta, S.; Mittra, K.; Dey, A. Photophysical and ligand binding studies of metalloporphyrins bearing hydrophilic distal superstructure. *J. Porph. Phthalocyanines* **2013**, *17*, 210. [CrossRef]
46. Samanta, S.; Mittra, K.; Sengupta, K.; Chatterjee, S.; Dey, A. Second Sphere Control of Redox Catalysis: Selective Reduction of O_2 to O_{2-} or H_2O by an Iron Porphyrin Catalyst. *Inorg. Chem.* **2013**, *52*, 1443. [CrossRef] [PubMed]
47. Mittra, K.; Chatterjee, S.; Samanta, S.; Sengupta, K.; Bhattacharjee, H.; Dey, A. A hydrogen bond scaffold supported synthetic heme Fe III–O 2− adduct. *Chem. Comm.* **2012**, *48*, 10535. [CrossRef] [PubMed]
48. Samanta, S.; Sengupta, K.; Mittra, K.; Bandyopadhyay, S.; Dey, A. Selective four electron reduction of O 2 by an iron porphyrin electrocatalyst under fast and slow electron fluxes. *Chem. Comm.* **2012**, *48*, 7631. [CrossRef]
49. Mandal, A.K.; Taniguchi, M.; Diers, J.R.; Niedzwiedzki, D.M.; Kirmaier, C.; Lindsey, J.S.; Bocian, D.F.; Holten, D. Photophysical Properties and Electronic Structure of Porphyrins Bearing Zero to Four meso-Phenyl Substituents: New Insights into Seemingly Well Understood Tetrapyrroles. *J. Phys. Chem. A* **2016**, *120*, 9719. [CrossRef]
50. Collman, J.P.; Gagne, R.R.; Halbert, T.R.; Marchon, J.C.; Reed, C.A. Reversible oxygen adduct formation in ferrous complexes derived from a picket fence porphyrin. Model for oxymyoglobin. *J. Am. Chem. Soc.* **1973**, *95*, 7868. [CrossRef]
51. Hartle, M.D.; Prell, J.S.; Plut, M.D. Spectroscopic investigations into the binding of hydrogen sulfide to synthetic picket-fence porphyrins. *Dalton Trans.* **2016**, *45*, 4843. [CrossRef]
52. Lindsey, J. Increased yield of a desired isomer by equilibriums displacement on binding to silica gel, applied to meso-tetrakis (o-aminophenyl) porphyrin. *J. Org. Chem.* **1980**, *45*, 5215. [CrossRef]
53. Gorlitzer, K.; Huth, S.; Jones, P.G. Color reaction of chlorhexidine and proguanil with hypobromite. *Pharmazie* **2005**, *60*, 269.
54. Guergueb, M.; Brahmi, J.; Nasri, S.; Loiseau, F.; Aouadi, K.; Guerineau, V.; Nasri, H. Zinc (II) triazole meso-arylsubstituted porphyrins for UV-visible chloride and bromide detection. Adsorption and catalytic degradation of malachite green dye. *RSC Adv.* **2020**, *10*, 22712. [CrossRef] [PubMed]
55. Chen, H.B.; Zeng, J.B.; Deng, X.; Chen, L.; Wang, Y.Z. Block phosphorus-containing poly (trimethylene terephthalate) copolyester via solid-state polymerization: Retarded crystallization and melting behaviour. *CrystEngComm.* **2013**, *15*, 2688–2698. [CrossRef]
56. Polster, J.; Lachmann, H. Spectrometric Titrations. Analysis of Chemical Equilibria. *Verlag Chemie* **1989**, *12*, 292.
57. Dumoulin, F.; Ahsen, V. Design and conception of photosensitisers. *J. Porph. Phthalocyanines* **2011**, *15*, 481. [CrossRef]
58. Brahmi, J.; Nasri, S.; Saidi, H.; Nasri, H.; Aouadi, K. Synthesis of new porphyrin complexes: Evaluations on optical, electrochemical, electronic properties and application as an optical sensor. *Chem. Select* **2019**, *14*, 1350. [CrossRef]
59. Ceyhan, T.; Altindal, A.; Erbil, M.; Bekaroglu, O. Synthesis, characterization, conduction and gas sensing properties of novel multinuclear metallo phthalocyanines (Zn, Co) with alkylthio substituents. *Polyhedron* **2006**, *25*, 7. [CrossRef]
60. Xue, X.; Tan, G. Effect of bivalent Co ion doping on electric properties of Bi0. 85Nd0. 15FeO3 thin film. *J. Alloys Compd.* **2013**, *575*, 90. [CrossRef]
61. Ghataka, S.; Ghosh, A. Observation of trap-assisted space charge limited conductivity in short channel MoS2 transistor. *App. Phys. Lett.* **2013**, *103*, 122103. [CrossRef]
62. Brahmi, J.; Nasri, S.; Saidi, H.; Aouadi, K.; Sanderson, M.R.; Winter, M.; Cruickshank, D.; Najmudin, S.; Nasri, H. Optical and photoelectronic properties of a new material: Optoelectronic application. *Comptes. Rendus. Chimie.* **2020**, *23*, 403. [CrossRef]

63. Al Mogren, M.M.; Ahmed, M.N.; Hasanein, A.A. Molecular modeling and photovoltaic applications of porphyrin-based dyes: A review. *J. Saudi. Chem. Soc.* **2020**, *24*, 303. [CrossRef]
64. Aloui, W.; Ltaief, A.; Bouazizi, A. Dielectrical properties of PET-MWCNT/P3HT: PC70BM/Al device: Impedance spectroscopy analysis. *Microelectron. Eng.* **2014**, *129*, 96–99. [CrossRef]
65. Mahmood, A.; Hu, J.Y.; Xiao, B.; Tang, A.; Wang, X.; Zhou, E. Recent progress in porphyrin-based materials for organic solar cells. *J. Mater. Chem. A.* **2018**, *6*, 16769. [CrossRef]
66. Opeyemi, O.; Louis, H.; Opara, C.; Funmilayo, O.; Magu, T. Porphyrin and Phthalocyanines-Based Solar Cells: Fundamental Mechanisms and Recent Advances. *Adv. J. Chem. Sect. A* **2019**, *2*, 21.
67. Fishchuk, I.I.; Kadashchuk, A.; Ullah, M.; Sitter, H.; Pivrikas, A.; Genoe, J.; Bassler, H. Electric field dependence of charge carrier hopping transport within the random energy landscape in an organic field effect transistor. *Phys. Rev. B.* **2012**, *86*, 045207. [CrossRef]

Disclaimer/Publisher's Note: The statements, opinions and data contained in all publications are solely those of the individual author(s) and contributor(s) and not of MDPI and/or the editor(s). MDPI and/or the editor(s) disclaim responsibility for any injury to people or property resulting from any ideas, methods, instructions or products referred to in the content.